Multidrug Resistance Protein MRP1 Reconstituted into Lipid Vesicles: Secondary Structure and Nucleotide-Induced Tertiary Structure Changes†

Liliana Manciu,‡ Xiu-Bao Chang,§ John R. Riordan,§ and Jean-Marie Ruysschaert*,‡

Laboratoire de Chimie-Physique des Macromolécules aux Interfaces (LCPMI), Université Libre de Bruxelles, B-1050 Brussels, Belgium, and S. C. Johnson Medical Research Center, Mayo Clinic Arizona, Scottsdale, Arizona 85259

Received May 8, 2000; Revised Manuscript Received July 21, 2000

ABSTRACT: Multidrug resistance protein MRP1 is an ATP-dependent drug efflux pump that confers resistance in human cancer cells to various chemotherapeutic drugs. We have reconstituted purified MRP1 in lipid vesicles. The reconstituted protein conserves ATPase and drug transport activity. Structural analysis of MRP1 was investigated by infrared spectroscopy for the first time. This technique offers a unique opportunity to determine structural parameters characterizing a membrane protein in its lipid environment. Addition of different ligands (MgATP, MgATPγS, MgADP and P_i, and MgADP) did not significantly affect the MRP1 secondary structure, which is made of 46% α-helix, 26% β-sheet, 12% β-turns, and 17% random coil. Binding of MgATP increased the protein accessibility to the solvent, suggesting a modification in the tertiary organization of the protein. Hydrolysis of MgATP to MgADP and P_i did not significantly change the global accessibility of the protein. Release of P_i, after hydrolysis, caused a decrease in the accessibility of MRP1 to the water phase which brings the protein back to its initial conformation. All together, the data demonstrate that MRP1 adopts different structures during its catalytic cycle.

Resistance of cells to cytotoxic agents is one of the major obstacles to the treatment of numerous cancers by chemotherapy. The intriguing point is that tumors exposed to a single cytotoxic agent frequently become cross-resistant to a broad spectrum of structurally and functionally unrelated compounds to which they have not been previously exposed. This phenomenon of cross-resistance to a wide spectrum of drugs is called multidrug resistance (MDR).[1] P-Glycoprotein (Pgp, 170 kDa) (*1*) and multidrug resistance protein (MRP1, 190 kDa) (*2*) have been identified on the plasma membrane of the resistant cells. These two proteins function as energy-dependent drug efflux pumps, and confer multidrug resistance by decreasing the intracellular concentration of drugs. Both proteins transport a wide range of drugs with different cellular targets. Transfection studies have confirmed that overexpression of either MRP1 or Pgp is sufficient to confer resistance to a similar but not identical spectrum of drugs (*3*−*5*). Whereas Pgp transports neutral and positively charged drugs in their unmodified form (*1*), *MRP1* overexpression is associated with an increased ATP-dependent glutathione *S*-conjugate transport activity (*6*). Experiments with inside-out membrane vesicles indicated that MRP1 is able to transport a range of substrates that are conjugated to glutathione (GSH), glucuronide, and sulfate. Well-known substrates are, for example, leukotrienes C_4, *S*-(2,4-dinitrophenyl)glutathione, 17-β-estradiol 17-(β-D-glucuronide), etoposide glucuronide, certain steroid glucuronides, and bile salts derivatives (*7*−*12*). MRP1 has also been proposed to catalyze the cotransport of several anticancer drugs such as vincristine and daunorubicin with glutathione (*13*−*15*).

Pgp and MRP1 share a similar core structure, consisting of 12 potential transmembrane segments in the C-proximal domain and two nucleotide binding domains (NBD1 and NBD2). However, MRP1 also contains a third NH_2-proximal domain of about 280 amino acids. Mutagenesis of potential N-glycosylation sites, limited proteolysis, and epitope insertion experiments suggest that the N-terminal domain comprises five transmembrane segments and that the NH_2 terminus is extracellular (*16*−*18*).

ATP binding and hydrolysis are essential for the proper functioning of MRP1, but the mechanism by which the energy derived from ATP hydrolysis is transduced into drug transport is not known. The mechanism of coupling ATP hydrolysis to drug transport is likely to involve substantial conformational changes in P-glycoprotein structure (*19*). Different conformational changes have previously been shown to take place during its catalytic cycle (*20*, *21*). Information about structural changes occurring during the catalytic cycle would be a first step in further understanding the mechanism used by MRP1 to transport its substrates

† This work was supported by the NIDDK of the National Institutes of Health, by the ARC (Action de Recherche Concertée, Belgium), and by the FRIA (Fonds pour l'Encouragement de la Recherche Scientifique dans l'Industrie et l'Agriculture) (to L.M.).

* To whom correspondence should be addressed: Laboratoire de Chimie Physique des Macromolécules aux Interfaces, Université Libre de Bruxelles, CP 206/2, Bd. du Triomphe, B-1050 Brussels, Belgium. Telephone: +30 2 6505377. Fax: +30 2 6505382. E-mail: jmruyss@ulb.ac.be.

‡ Université Libre de Bruxelles.

§ Mayo Clinic Arizona.

[1] Abbreviations: MDR, multidrug resistance; MRP1, multidrug resistance protein; Pgp, P-glycoprotein; NBD, nucleotide binding domain; ATR, attenuated total reflection; FTIR, Fourier transform infrared spectroscopy; H−D, hydrogen−deuterium; DDM, *n*-dodecyl β-D-maltoside; GSH, glutathione; LTC_4, leukotrienes; P_i, inorganic phosphate; V_i, orthovanadate; ATPγS, adenosine 5′-*O*-(3-thiotriphosphate); AMP, adenosine 5′-monophosphate; CHAPS, 3-[(3-cholamidopropyl)dimethylammonio]-1-propanesulfonate.

10.1021/bi001043v CCC: $19.00
Published on Web 09/30/2000

across the biological membrane. Histidine-tagged MRP1 was recently overexpressed in transfected hamster cells and purified using Ni^{2+}-chelate chromatography (*22*). In the study presented here, we describe the efficient reconstitution of purified MRP1 in lipid vesicles. The reconstituted protein conserves ATPase and transport activity. Attenuated total reflection (ATR) Fourier transform IR spectroscopy was used to obtain information about the structure of MRP1 in its lipidic environment (*23*−*25*). Hydrogen−deuterium exchange kinetics measurements and fluorescence quenching experiments were used to investigate tertiary structure changes in the presence of specific ligands of MRP1 such as MgATP, MgATPγS, MgADP and P_i, and MgADP.

This study indicates that the secondary structure of MRP1 is not affected upon binding of different nucleotides. In contrast, the tertiary structure of MRP1 changes during the catalytic cycle.

EXPERIMENTAL PROCEDURES

Chemicals. Asolectin (soybean phospholipids; Sigma) was purified according to the method of Kagawa and Racker (*26*) and stored at −20 °C in chloroform. [^{3}H]LTC_4 (146 Ci/mmol) was a Dupont NEN product. D_2O was from Merck. ATP, ADP, ATPγS, and *n*-dodecyl β-D-maltoside were from Sigma. CHAPS was from Boehringer Mannheim. SM2 Bio-Beads were from Bio-Rad. Nitrocellulose filters were purchased from Orange Scientific, and His·Bind Resin was from Novagen.

Purification. The purification of MRP1 was carried out as described previously (*22*) with some modifications, including the omission of excess phospholipids. Membrane vesicles, containing overexpressed MRP1, were solubilized in buffer A [20 mM Tris-HCl (pH 7.9) containing 500 mM NaCl, 5 mM imidazole, 1% (w/v) *n*-dodecyl β-D-maltoside (DDM), and 20% (v/v) glycerol]. The sample was sonicated, and insoluble material was removed by centrifugation at 10000*g* for 15 min. The supernatant was applied onto a His·Bind Resin column (Novagen), which was pre-equilibrated in buffer A. The column was washed with 6 column volumes of buffer A containing 0.5% DDM and 25 mM imidazole, followed by a second wash with 6 column volumes of buffer A containing 0.1% DDM, 10% glycerol, and 40 mM imidazole. The column was washed one more time with 6 column volumes of 20 mM Tris-HCl (pH 7.4) containing 500 mM NaCl, 0.1% DDM, and 40 mM imidazole. The protein was eluted with 2 column volumes of 20 mM Tris-HCl (pH 7.4) containing 0.1% DDM, 0.05% β-mercaptoethanol, and 300 mM imidazole. The eluate was dialyzed extensively against 50 volumes of 5 mM Tris-HCl (pH 7.4), 500 mM NaCl, 0.05% DDM, and 0.05% β-mercaptoethanol in the cold room.

Reconstitution of MRP1. A film of asolectin (10 mg) was formed by evaporation of choroform under a stream of N_2, followed by overnight drying under vacuum. Liposomes were prepared by sonication of the lipid film (7 min, on a 250 W Vibra Cell Sonifier) in 1.37 mL of 20 mM Tris-HCl, 75 mM NaCl, 0.5 mM EDTA, and 1 mM DTT (pH 7.4). The sonicated phospholipid solution (130 μL) was added in 750 μL (final volume) of reconstitution buffer containing DDM [1/0.7 (w/w) lipid/detergent ratio]. The mixture was incubated for 20 min at 4 °C, while being stirred continuously. Purified protein, dissolved in 0.1% DDM, was added to lipid/detergent mixed micelles, at a 1/20 (w/w) protein/lipid ratio, and the volume was adjusted to 1 mL with reconstitution buffer. The detergent/protein/phospholipid mixture was gently stirred for 20 min at 4 °C, and the detergent was removed by adding SM_2 Bio-Beads (previously washed with methanol and MilliQ water).

The supernatant collected from SM_2 Bio-Beads was mixed with an equal volume of 80% sucrose and overlaid with a 30 to 10% sucrose linear gradient. After an overnight centrifugation at 120000*g* and 4 °C in a Beckman L7 ultracentrifuge with a SW60 rotor, the gradient was fractionated from the bottom of the tube. The phospholipids and protein distribution were measured by the enzymatic colorimetric assay of phosphatidylcholine (Boerhinger Mannheim) and by tryptophan fluorescence ($\lambda_{excitation} = 280$ nm and $\lambda_{emission} = 330$ nm).

ATPase Activity. The ATPase activity of proteoliposomes was measured according to the procedure described by Shapiro and Ling (*27*). The protein content of the samples was determined by the method of Peterson (*28*).

Transport Assays. Standard transport assays were carried out at 37 °C in a 130 μL volume containing 10 μg of reconstituted MRP1, 4 mM ATP, 10 mM $MgCl_2$, and 50 nM [^{3}H]LTC_4 in 20 mM Tris-HCl (pH 7.4). Aliquots of 25 μL were removed from the incubation mixture, and uptake was stopped by rapid dilution in 1 mL of ice-cold transport buffer [20 mM Tris-HCl (pH 7.4) and 10 mM $MgCl_2$], followed by filtration through nitrocellulose filters (0.025 μm pore size). Filters were immediately washed twice with 5 mL of cold transport buffer and air-dried. The amount of vesicle-associated radioactivity was measured in 10 mL of scintillation liquid. In control experiments, MgATP was replaced with 4 mM MgAMP. The rate of ATP-dependent uptake was calculated by subtracting values obtained in the presence of MgAMP as a blank from those obtained in the presence of MgATP.

Infrared Spectroscopy. (1) Sample Preparation. The proteoliposomes containing MRP1 were isolated on a sucrose gradient and then pelleted by centrifugation twice in 2 mM Hepes buffer (pH 7.4). This step allows elimination of sucrose whose spectrum interferes with the IR analysis. The sample (containing 20 μg of reconstituted protein) was resuspended in 50 μL of 2 mM Hepes buffer (pH 7.4) and was spread and slowly evaporated under a N_2 flux on one side of the ATR plate (*29*). The internal reflection element was a germanium ATP plate (50 mm × 20 mm × 2 mm, Harrick EJ2121) with an aperture angle of 45°, yielding 25 internal reflections.

(2) Secondary Structure Analysis. The sample on the ATR plate was deuterated by flushing D_2O-saturated N_2 for 2 h. The H−D exchange allows differentiation of the α-helix from random coil, whose absorption band shifts from 1655 to ∼1642 cm^{-1} (*30*). Attenuated total reflection infrared (ATR-FTIR) spectra were recorded on a Bruker spectrophotometer at a resolution of 2 cm^{-1}. Five hundred twelve scan cycles were averaged from each measurement. In each cycle, the sample spectra were ratioed against the average of the background spectra of a clean germanium plate. The spectrophotometer was continuously purged with dry air. The determination of the protein secondary structure was carried out by analysis of the deuterated amide I band as described

previously (*23*, *24*, *29*, *30*). The frequency limits for the different structures were as follows: 1662−1645 cm^{-1} for α-helix, 1689−1682 and 1637−1613 cm^{-1} for *β*-sheet, 1682−1662.5 cm^{-1} for *β*-turns, and 1644.5−1637 cm^{-1} for unordered structures. The combination of resolution enhancement methods with a band fitting procedure allows the assessment of the protein secondary structure (α-helix, *β*-sheet, *β*-turns, and unordered structures).

Hydrogen−Deuterium Exchange Kinetics. Films containing 20 *μ*g of reconstituted protein were prepared as described above. Nitrogen gas was saturated with D_2O (by bubbling through a series of five vials containing D_2O) at a flow rate of 75 mL/min (controlled by a Brooks flow meter). Before the exchange was started, 10 spectra of the sample dried on the ATR plate were recorded to verify the stability of the measurement and the reproducibility of the area determination. At time zero, the tubing was connected to the cavity of the sealed chamber surrounding the film. For each kinetic time point, 24 spectra were recorded and averaged at a resolution of 2 cm^{-1} for each kinetic time point. At the beginning of the kinetic measurements, spectra were recorded every 30 s. After the first 10 min, the time interval was logarithmically increased. After 20 min, the interval between the scans was large enough to allow the interdigitation of a second kinetic program. A second sample placed on another ATR setup of the Bruker sample shuttle was then analyzed with the same time sampling with a 20 min offset by connecting the D_2O-saturated N_2 flow in series with the first sample. From this time on, our program changed the shuttle position to follow the two kinetic programs (*23*, *31*). Typically, one of the samples placed on the shuttle was prepared in the absence of a substrate and the other in the presence of a substrate as indicated. A background deuteration kinetic spectrum recorded with the same germanium plate at the same position in the sample shuttle but in the absence of the sample was subtracted from the kinetic spectrum recorded in the presence of the sample. The atmospheric contribution was also recorded and subtracted from each spectrum. Indeed, even though the spectrophotometer was purged with dry air for 10 min before the experiment was started, further removal of traces of water vapor took place for several hours, superimposing distinct sharp bands from the water vapor onto the protein spectra (*32*).

For each spectrum, the area of amide II was divided by the corresponding amide I area. This permitted us to take into account any variations in the total intensity of the spectra due in part to the presence of D_2O, which causes swelling of the sample layer and therefore increases the average distance between the protein sample and the germanium crystal surface. Since the ATR spectrum intensity depends on this distance (*24*), this results in a loss of a few percent of the band intensity for all measured bands. The integration of the amide II and amide I areas was performed with a baseline drawn between limits corresponding to the local minima of the spectrum. The amide II/amide I ratio, expressed between 100 and 0%, was plotted versus deuteration time. The 100% value is defined by the amide II/amide I ratio obtained before deuteration, whereas the 0% value corresponds to zero absorption in the amide II region (*25*, *33*).

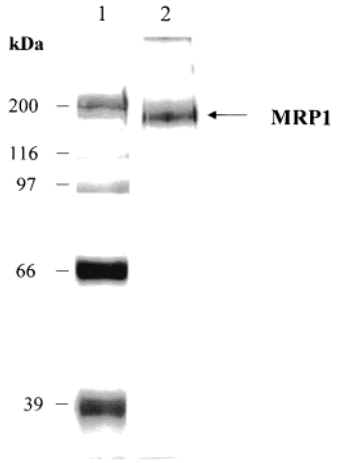

FIGURE 1: SDS−PAGE gel (silver-stained) of purified MRP1. Lane 1 contained the high-range markers (the molecular masses of the standards are indicated in kilodaltons). Purified MRP1 (1.5 *μ*g) was loaded in lane 2. The arrow indicates the position of MRP1.

Fluorescence Quenching. Acrylamide quenching experiments were carried out on an SLM Aminco 8000 spectrofluorometer at room temperature. Samples were stirred continuously in a 1.0 cm × 1.0 cm quartz cuvette. The excitation wavelength was set at 290 nm instead of 280 nm to reduce the absorbance of acrylamide. The fluorescence was monitored at 334 nm. Increasing amounts of acrylamide were added from a 3 M stock solution to the proteoliposome suspension (1 mL in water) containing 7 *μ*g of reconstituted MRP1 and various ligands. The final concentration for the different ligands was 3 mM. The acrylamide concentration was from 0 to 0.08 M. Above this concentration, the static quenching by acrylamide is responsible for the deviation from linearity in the Stern−Volmer plots. The quenching data were plotted according to the Stern−Volmer equation (*34*):

$$F_0/F = 1 + K_{sv}[Q] \quad (1)$$

where F_0 and F are the fluorescence intensities in the absence and presence of the acrylamide, respectively, [Q] is the concentration of acrylamide, and K_{sv} is the Stern−Volmer constant.

RESULTS

Purification and Reconstitution of MRP1. Histidine-tagged recombinant MRP1 was purified from transfected hamster cells by Ni^{2+}-chelate chromatography, as described in Experimental Procedures. The silver-stained SDS−PAGE gel of the protein that eluted from the Ni^{2+}-chelate column exhibits a major band at approximately 190 kDa which corresponds to the monomer of MRP1 (Figure 1). Aside from this band, the only significant additional band present in the final preparation has a molecular mass corresponding to a homodimer. This band is detectable with a specific monoclonal antibody (MRPr1) (data not shown). Analysis of this gel by densitometry demonstrates that MRP1 is approximately 99% pure.

Purified MRP1 was mixed with DDM-destabilized asolectine liposomes. Subsequently, DDM was removed by adsorption on polystyrene beads, as described in Experimental Procedures.

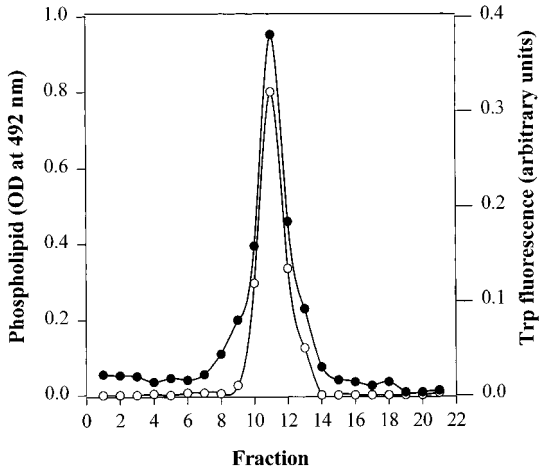

FIGURE 2: Sucrose gradient profile of MRP1-containing vesicles. After centrifugation, fractions were collected from the bottom to the top of the gradient and measured for protein (●) and lipid (○) content as described in Experimental Procedures.

Proteoliposomes were layered on the bottom of a linear sucrose gradient, and after centrifugation, the gradient was fractionated from the bottom of the tube (Figure 2). Comigration of lipids and MRP1 (fractions 10−13) along the sucrose gradient demonstrates that proteoliposomes have been formed. The distribution of MRP1 within the liposomes was quite homogeneous since one population of proteoliposomes was detected. No protein aggregates were detected at the bottom of the gradient (fraction 1, Figure 2), indicating that all MRP1 was inserted into the liposomes during reconstitution. The fractions containing proteoliposomes were pooled and washed by centrifugation in 2 mM Hepes (pH 7.4), at 160000*g* and 4 °C for 2 h. Fifty percent of the protein was recovered. The proteoliposomes were formed at a 1/28 (w/w) protein/lipid ratio with a diameter of about 200 nm as determined by light scattering (not shown).

ATPase Activity and Orientation of Reconstituted MRP. The specific ATPase activity of MRP1 reconstituted in liposomes was about 10 ± 2 nmol min^{-1} (mg of protein)$^{-1}$. The orientation of MRP1 incorporated in proteoliposomes was determined using the CHAPS permeabilization method of Sharom et al. (*35*), based on the measure of the ATPase activity in the presence and in the absence of CHAPS. The ATPase activity of reconstituted MRP1 was not increased by addition of 2 mM CHAPS; this CHAPS concentration was previously shown to permeabilize the proteoliposomes (*35*, *36*). This result indicates that MRP1 is inserted into the liposomes in an inside-out configuration with its catalytic sites pointing outside the liposomes and that the reconstituted protein retains enzymatic activity. The ATPase activity of the reconstituted MRP is 1.6-fold stimulated by addition of 20 μM daunorubicin in the presence of 2.5 mM GSH. The same level of activation has been measured using plasma membrane vesicles (*37*).

Transport Assays. LTC_4 was previously shown to be an MRP1 substrate in multidrug-resistant cells expressing the protein (*8*, *9*). The transport function of the MRP1 was assayed by assessing the ATP-dependent accumulation of [^{3}H]LTC_4 in membrane vesicles isolated from MRP1-expressing cells (*8*, *9*). We have performed similar assays using purified MRP1 reconstituted into proteoliposomes. Proteoliposomes containing MRP1 were incubated with [^{3}H]-

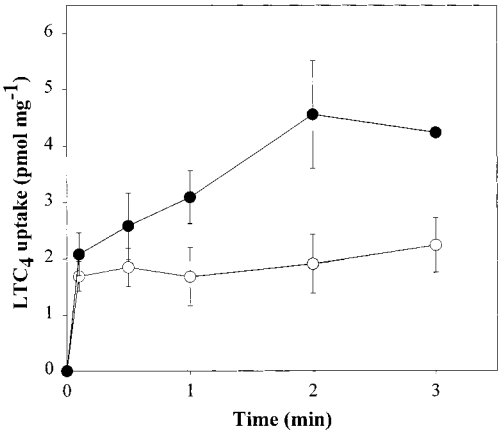

FIGURE 3: Time-dependent uptake of [^{3}H]LTC_4 into proteoliposomes. Proteoliposomes containing 10 μg of MRP1 were incubated for the indicated times in the presence of 50 nM [^{3}H]LTC_4 at 37 °C as described in Experimental Procedures. White (○) and black (●) symbols represent uptake in the presence of 4 mM MgAMP and in the presence of 4 mM MgATP, respectively. Data points represent means ± the standard deviation from three experiments. The absence of error bars means that the standard deviation is smaller than the symbol.

LTC_4 (50 nM), and the rate of uptake of LTC_4 into the vesicles was determined in the presence of 4 mM MgATP and 4 mM MgAMP. In the presence of MgAMP, the uptake corresponds to passive diffusion and partitioning into the lipid bilayer of LTC_4. The difference between the level of LTC_4 accumulation in the presence of 4 mM MgATP and 4 mM MgAMP was considered to represent the fraction that is transported in an ATP-dependent process and accumulates in the aqueous phase. The level of accumulation of LTC_4 into the proteoliposomes was about 2-fold higher in the presence of MgATP than in the presence of MgAMP (Figure 3), indicating that reconstituted MRP1 is able to transport LTC_4 in an ATP-dependent manner.

Secondary Structure Analysis. The secondary structure of MRP1 was investigated by attenuated total reflection infrared spectroscopy (ATR-FTIR). The method is based on the analysis of the "amide I" (1700−1600 cm^{-1}) band attributed to the ν(C═O) of the peptide bond, and extremely sensitive to the secondary structure of the proteins (*23*, *24*, *29*).

IR spectra of MRP1 were recorded in the absence and presence of different nucleotides: MgATP, MgATPγS, MgADP, and MgADP and P_i. MgATPγS is a nonhydrolyzable MgATP analogue, which allows discrimination between the influence of nucleotide binding and nucleotide hydrolysis on MRP1 structure. MgADP and P_i and MgADP allow study of the conformational changes at two different steps of the catalytic cycle.

The shape of the deuterated amide I band of all the spectra was not significantly modified upon addition of any of these nucleotides (data not shown). A quantitative analysis of the amide I band by Fourier deconvolution and curve fitting, as described previously (*23*, *30*), confirms that nucleotide binding had little effect on the secondary structure of MRP1 (Table 1).

Kinetics of Deuteration. The kinetics of deuteration is a function of both the secondary structure existing within the protein (the exchange is faster in nonordered structures than in highly organized structures such as α-helices and β-sheets involving hydrogen bonds) and the accessibility of the NH

Table 1: Secondary Structure of MRP1 Determined in the Absence and in the Presence of Different Nucleotides[a]

ligand	α-helix (%)	β-sheet (%)	β-turn (%)	random coil (%)
none	46 ± 2	26 ± 3	11 ± 2	17 ± 1
MgATPγS[b]	42 ± 1	28 ± 1	12 ± 1	17 ± 1
MgATP[b]	45 ± 1	27 ± 1	12 ± 1	17 ± 1
MgADP and P_i[b]	44 ± 1	27 ± 1	10 ± 2	17 ± 1
MgADP[b]	43 ± 1	28 ± 3	12 ± 2	16 ± 1

[a] The percentages were obtained by analysis of the shape of the amide I band according to Goormaghtigh et al. (*29*). Data represent mean values ± the standard deviation from three experiments. [b] MRP1/nucleotide molar ratio of 1/6.

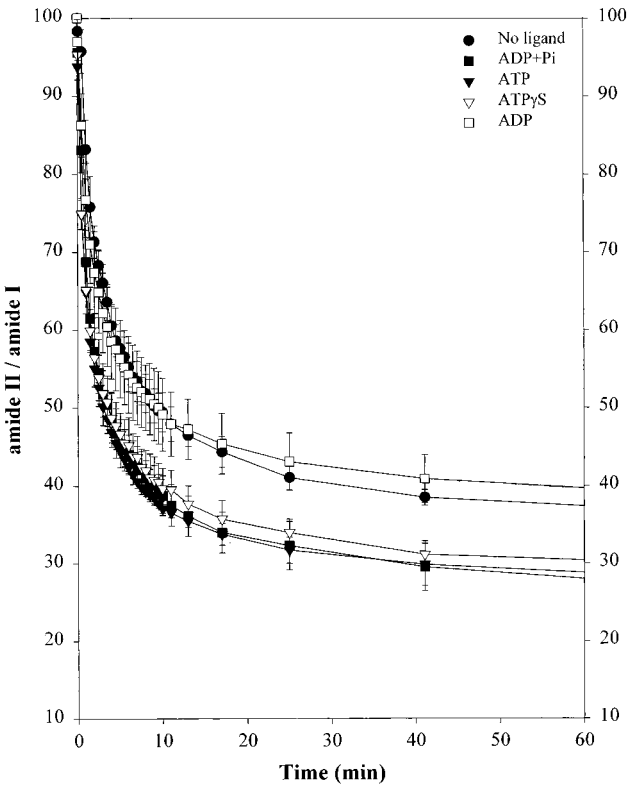

FIGURE 4: Evolution of the proportion of exchanged amide bonds computed between 0 and 100% as described in Experimental Procedures as a function of the deuteration time: (●) no ligand added, (▽) MgATPγS, (▼) MgATP, (■) MgADP and P_i, and (□) MgADP. The MRP/nucleotide molar ratio was 1/6. The curves are the means of three experiments. The error bars represent the standard deviation.

groups to the aqueous medium depending on its tertiary structure. Since we showed that the secondary structure of MRP1 did not change in the presence of various nucleotides, the rate of H−D exchange can be used as an indicator of tertiary structure changes. The kinetics of H−D exchange is followed by monitoring the area of the amide II band as a function of the time of exposure to D_2O. The decrease of the amide II area is shown as a function of deuteration time in Figure 4.

It appears from Figure 4 that the H−D exchange rate is higher in the presence of MgATPγS, MgATP, and MgADP and P_i than for the protein alone or in the presence of MgADP.

It has been shown that phosphate binding to Pgp occurs with a relatively weak affinity (*38*). We conducted a control experiment using MgATP and vanadate, to make sure that phosphate binds to the protein in the case of the MRP1·MgADP·P_i intermediate. Vanadate was previously shown to be a phosphate analogue that bound to the phosphate binding sites in myosin (*39*) and Pgp (*38*, *40*). Recent crystal structures of the catalytic domain confirm that the ADP−vanadate complex resembles the ADP and phosphate-bound catalytic intermediate (*41*, *42*). The exchange rates obtained in the presence of MgATP and V_i and in the presence of MgADP and P_i were identical (data not shown).

Table 2: Proportion (a_1−a_3) of the Three Exponential Components Characterized by Half-Decays of $T_1 = 1$ min, $T_2 = 9$ min, and $T_3 = 666$ min[a]

ligand	a_1 (%)	a_2 (%)	a_3 (%)
none	30 (459)	34 (521)	39 (597)
MgATPγS	42 (643)	21 (322)	33 (505)
MgATP	44 (674)	22 (337)	31 (475)
MgADP and P_i	43 (658)	26 (398)	31 (475)
MgADP	33 (505)	24 (367)	43 (658)

[a] Numbers in parentheses are the number of amino acid residues involved.

Hydrogen atoms with different exchange rates are implicated in the exchange process. Because H−D exchange is a first-order reaction, the exchange curve is expected to display a multiexponential decay corresponding to the different groups, *i*, of amide protons characterized by a common period T_i

$$H(t) = \sum_i a_i \exp(-t/T_i) \qquad (2)$$

where a_i is the proportion of the group *i*. A nonlinear fitting of all the experimental curves of Figure 4, without contraints on the periods T_i and on the proportions a_i, yields three periods (T_1−T_3). To compare the proportions a_i of each amide group for the different curves, a second fitting was performed by setting the T_i to their average value ($T_1 = 1$, $T_2 = 9$, and $T_3 = 666$ min). Results of this analysis are reported in Table 2.

In the absence of ligand, approximately 30% of the amide hydrogen is exchanged within 1 min of exposure to deuterium and an additional 34% after 9 min. About 39% of the amide hydrogen bonds of MRP1 exchange very slowly ($T_3 = 666$ min), reflecting a poor accessibility to the aqueous medium. Addition of MgATPγS, MgATP, or MgADP and P_i (1/6 MRP1/nucleotide molar ratio) results in an increase of about 12% (200 amino acid residues) of the population of fast exchanged amino acids, concomitant with a decrease in the fraction of intermediate and slowly exchanging amide protons.

In the presence of MgADP (1/6 MRP1/MgADP molar ratio), the percentage of fast exchanging amide protons is similar to that observed for the protein alone, but the fractions of intermediate and slowly exchanging amide protons are different.

Fluorescence Quenching. Fluorescence experiments carried out in the presence of ligand can also indicate the existence of conformational changes arising from ligand binding. MRP1 contains 30 tryptophan residues; 10 of them are predicted to be associated with transmembrane domains and 20 with extramembrane domains. Tryptophan quenching experiments were therefore performed in the absence and presence of MgATPγS, MgATP, MgADP and P_i, and MgADP (3 mM final concentration). The extent of tryp-

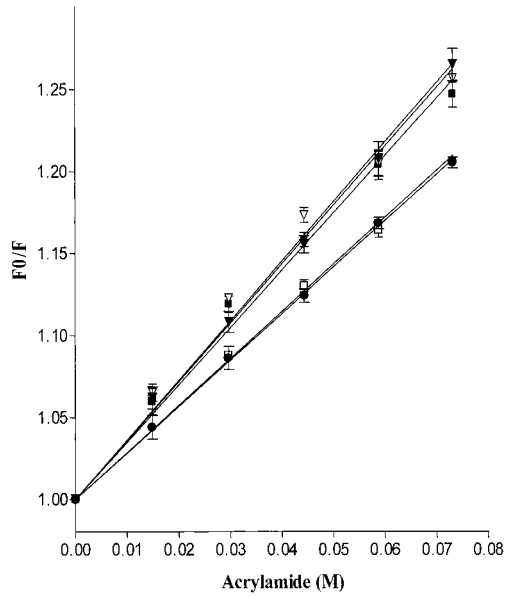

FIGURE 5: Stern−Volmer plots of MRP1 tryptophan quenching by acrylamide in the absence and presence of nucleotides. F is the measured fluorescence intensity, and F_0 is the initial fluorescence intensity in the absence of acrylamide: (●) no ligand added, (▽) 3 mM MgATPγS, (▼) 3 mM MgATP, (■) 3 mM MgADP and P_i, and (□) 3 mM MgADP. The results are the means of three experiments. The error bars represent the standard deviation.

Table 3: Influence of Nucleotides Binding on the Stern−Volmer Constants (K_{sv})[a]

ligand	K_{sv} (M^{-1})[b]
none	2.84 ± 0.04
MgATP	3.59 ± 0.06
MgATPγS	3.63 ± 0.07
MgADP and P_i	3.50 ± 0.07
MgADP	2.86 ± 0.06

[a] Nucleotide concentrations of 3 mM were used in all cases. [b] K_{sv} values were determined from the slope of Stern−Volmer plots of the type shown in Figure 5 for MRP1 in the absence and presence of different ligands. Three independent experiments were carried out, and K_{sv} values were generated by computer fitting.

tophan exposure to the solvent was subsequently determined by continuously monitoring the MRP1 fluorescence intensity in the presence of increasing concentrations of acrylamide (0−0.08 M), a neutral aqueous quencher. Figure 5 shows the effects of acrylamide on tryptophan fluorescence intensity and reveals similar quenching profiles for the protein alone or in the presence of MgADP, whereas upon addition of MgATPγS, MgATP, and MgADP and P_i, the quenching is more pronounced, which suggests an increase in the tryptophan accessibility to the aqueous environment. The Stern−Volmer constants, K_{sv}, were determined in each case (Table 3).

DISCUSSION

The mechanism by which MRP1 mediates drug efflux from resistant cells is not understood. Information about the secondary structure and changes in the tertiary structure upon binding of different ligands could help to further progress in the understanding of this mechanism. Because of the complexity of the biological membrane, an absolute prerequisite before any structural investigation was to purify and reconstitute the protein in its active form in lipid vesicles. Histidine-tagged recombinant MRP1 was purified from transfected hamster cells by Ni^{2+}-chelate chromatography, as described previously (*22*). We describe here a method of reconstitution of purified MRP1 in lipid vesicles which yields proteoliposomes with a 1/28 (w/w) protein/lipid ratio. A significant MRP1 concentration is indeed required for further infrared spectroscopic investigations. The reconstituted MRP1 exhibited ATPase activity which can be modulated by drugs and ATP-dependent LTC_4 transport. The basal ATPase activity of MRP1 is lower than that of P-glycoprotein (*27*, *35*) but is comparable to that reported by Mao et al. (*43*) for MRP1 purified from multidrug resistant H69AR lung cancer cells by immunoaffinity chromatography. More importantly, the MRP activity associated with the proteoliposomes is quite similar to that found in membrane vesicles prepared from plasma membranes (*43*).

The proportions of different secondary structure elements of MRP1, estimated by ATR-FTIR, were 46% α-helix, 26% β-sheet, 12% β-turn, and 17% random coil (Table 1). When the generally accepted topology of MRP1 with 17 putative transmembrane α-helices (*16*, *18*, *44*, *45*) is considered, representing 22% of the protein, our data suggest that extramembrane α-helices (in the three large cytoplasmic domains, for example) or additional transmembrane helical segments exist within the protein. Analysis of the amide I band by Fourier self-deconvolution and curve fitting (Table 1) indicates that the secondary structure of MRP1 is not significantly affected by the presence of MgATPγS, MgATP, MgADP and P_i, or MgADP. Other ATPases reconstituted in lipid vesicles, such as *Neurospora* plasma membrane H^+-ATPase and Pgp, have been shown previously not to be affected in their secondary structure after binding of specific ligands (*19*, *31*).

The rate of H−D exchange was used here to evaluate changes in the accessibility of the protein to the aqueous phase in the presence of various ligands. Comparison of ATR-FTIR experiments carried out on films with data obtained in solution by NMR has demonstrated the validity of this approach (*33*).

H−D exchange measurements provide evidence that about 39% of the total amino acid content of the protein is poorly accessible to the aqueous medium. These slowly exchanging amino acids are characterized by a half-decay T_3 of 666 min. The presence of this amide population, characterized by a very low exchange rate, could be due, in part, to the shielding effect of the membrane. Transmembrane domains of several membrane proteins, such as glycophorin and bacteriorhodopsin, are inaccessible to the solvent as shown by their slow kinetics of H−D exchange (*46*, *47*). The slowly exchanging amide protons of MRP1 could therefore be formed by a core of amino acids located within the membrane. However, according to the protein sequence, the predicted transmembrane domains of MRP1 account for only 22% of the total amino acids (*16*, *18*, *44*, *45*). A certain proportion of the slowly exchanging amino acids must therefore be located outside the membrane where they are folded into structured domains.

Addition of MgATPγS, MgATP, or MgADP and P_i increases the accessibility to the water phase of at least 200 amino acid residues (Table 2). In the presence of MgADP, the H−D exchange rate is similar to that of the protein alone. However, Table 2 shows that although the global exchange

is the same, the population of the amide protons exchanging at intermediate rate is decreasing significantly, concomitant with an increase in the population of the amide protons exchanging at a slow rate. This means that MgADP modifies the MRP1 structural organization, but that these changes cannot be detected on the experimental exchange curves. Binding of MgATPγS leads to a reorganization of the hydrogen bonds resulting in an increase in the accessibility of the MRP1 domains to the solvent. These measurements do not allow location of the domains involved in the H−D exchange or estimation of the contribution of amino acids belonging to transmembrane segments. The accessibility is not modified after ATP hydrolysis, when P_i is still associated with the protein. Indeed, H−D experiments conducted with MgATP and V_i allow us to mimick the transition state conformation of the normal reaction pathway intermediate (MRP1·MgADP·P_i). Release of P_i brings the structure back to that of MRP1 alone.

Fluorescence quenching experiments confirm the existence of a conformational change in MRP1 in the presence of MgATPγS, MgATP, or MgADP and P_i, resulting in an increased solvent accessibility of its tryptophan residues.

The interpretation of the H−D exchange kinetics reported here in terms of tertiary structure changes in MRP1, despite the absence of secondary structure changes, requires a careful examination of the data. Even if the secondary structures are not significantly affected by addition of ligands, their stability can be modified. This would have a significant effect on the exchange rate. However, modifications of the stability of secondary structures involve modifications in the strength of hydrogen bonds, and this causes modifications in the amide I and amide II regions (*23*). Analysis of the FTIR spectra of MRP1 indicates that such changes did not take place upon addition of ligands.

Previous studies, including IR spectroscopy (*20*), fluorescence quenching measurements (*19*, *48*), and limited trypsine digestion (*21*), have demonstrated that Pgp tertiary structure changes during the hydrolysis cycle and four conformational states have been identified. The data accumulated here indicate that during the MRP1 catalytic cycle, its secondary structure is not modified but tertiary structure changes do occur. The environment of 10−13% of the amino acid residues of MRP1 is modified when the protein binds and hydrolyzes MgATP to MgADP and P_i. Release of P_i restores the initial MRP1 conformation. It may seem surprising that only two conformational states associated with the MRP1 catalytic cycle were identified as compared to Pgp. It should, however, be stressed that the kinetics of exchange of MRP1 is much faster than for Pgp and that there is a possibility that additional intermediate states may not have been detected using the approach described here. We recently demonstrated that the shift of the amide I occurring during the H−D exchange process can be used to define the contribution of each secondary domain (α-helix, β-sheet, random, and β-turn) to the global exchange (*49*, *50*). Work is in progress in our laboratory to take advantage of this property to detect new structural changes involved in transport by MRP1.

REFERENCES

1. Gottesman, M. M., and Pastan, I. (1993) *Annu. Rev. Biochem. 62*, 385−427.
2. Cole, S. P. C., Bhardwaj, G., Gerlach, J. H., Mackie, J. E., Grant, C. E., Almquiste, K. C., Stewart, A. J., Kurz, E. U., Duncan, A. M. V., and Deeley, R. G. (1992) *Science 258*, 1650−1654.
3. Cole, S. P. C., Sparks, K. E., Fraser, L., Loe, D. W., Grant, C. E., Wilson, G. M., and Deeley, R. G. (1994) *Cancer Res. 54*, 5902−5910.
4. Grant, C. E., Valdirmasson, G., Hipfner, D. R., Almquist, K. C., Cole, S. P. C., and Deeley, R. G. (1994) *Cancer Res. 54*, 357−361.
5. Zaman, G. J., Flens, M. J., van Leusden, M. R., de Haas, M., Mulder, H. S., Lankelma, J., Pinedo, H. M., Scheper, R. J., Baas, F., Broxterman, H. J., and Borst, P. (1994) *Proc. Natl. Acad. Sci. U.S.A. 91*, 8822−8826.
6. Jedlitschky, G., Leier, I., Buchholz, U., Center, M., and Keppler, D. (1994) *Cancer Res. 54*, 4833−4836.
7. Leier, I., Jedlitschky, G., Buchholz, U., Cole, S. P. C., Deeley, R. G., and Keppler, D. (1994) *J. Biol. Chem. 269*, 27807−27810.
8. Leier, I., Jedlitschky, G., Buchholz, U., and Keppler, D. (1994) *Eur. J. Biochem. 220*, 599−606.
9. Loe, D. W., Almquist, K. C., Deeley, R. G., and Cole, S. P. C. (1996) *J. Biol. Chem. 271*, 9675−9682.
10. Loe, D. W., Almquist, K. C., Cole, S. P. C., and Deeley, R. G. (1996) *J. Biol. Chem. 271*, 9683−9689.
11. Müller, M., Meijer, C., Zaman, G. J. R., Borst, P., Scheper, R. J., Mulder, N. H., de Vries, E. G. E., and Jansen, P. L. M. (1994) *Proc. Natl. Acad. Sci. U.S.A. 91*, 13033−13037.
12. Jedlitschky, G., Leier, I., Buchholz, U., Barnouin, K., Kurz, G., and Keppler, D. (1996) *Cancer Res. 56*, 988−994.
13. Loe, D. W., Deeley, R. G., and Cole, S. P. C. (1998) *Cancer Res. 58*, 5130−5136.
14. Rappa, G., Lorico, A., Flavell, R. A., and Sartorelli, A. C. (1997) *Cancer Res. 57*, 5232−5237.
15. Renes, J., de Vries, E. G., Nienhuis, E. F., Jansen, P. L., and Muller, M. (1999) *Br. J. Pharmacol. 126*, 681−688.
16. Bakos, E., Hegedüs, T., Hollo, Z., Welker, E., Tusnady, G. E., Zaman, G. J., Flens, M. J., Varadi, A., and Sarkadi, B. (1996) *J. Biol. Chem. 271*, 12322−12326.
17. Hifner, D. R., Almquist, K. C., Lesli, E. M., Gerlach, J. H., Grant, C. E., Deeley, R. G., and Cole, S. P. C. (1997) *J. Biol. Chem. 272*, 23623−23630.
18. Kast, C., and Gros, P. (1998) *Biochemistry 37*, 2305−2313.
19. Liu, R., and Sharom, F. J. (1996) *Biochemistry 35*, 11865−11873.
20. Sonveaux, N., Shapiro, A. B., Goormaghtigh, E., Ling, V., and Ruysschaert, J. M. (1996) *J. Biol. Chem. 271*, 24617−24624.
21. Wang, G., Pincheira, R., and Zhang, J. T. (1997) *Biochem. J. 328*, 897−909.
22. Chang, X. B., Hou, Y. X., and Riordan, J. (1997) *J. Biol. Chem. 272*, 30962−30968.
23. Goormaghtigh, E., Cabiaux, V., and Ruysschaert, J. M. (1994) *Subcell. Biochem. 23*, 329−450.
24. Goormaghtigh, E., Raussens, V., and Ruysschaert, J. M. (1999) *Biochim. Biophys. Acta 1422*, 105−185.
25. Raussens, V., Narayanaswami, V., Goormaghtigh, E., Ryan, R. O., and Ruysschaert, J. M. (1996) *J. Biol. Chem. 271*, 23089−23095.
26. Kagawa, J., and Racker, E. (1971) *J. Biol. Chem. 246*, 5477−5487.
27. Shapiro, A. B., and Ling, V. (1994) *J. Biol. Chem. 269*, 3745−3754.
28. Peterson, G. L. (1977) *Anal. Biochem. 83*, 346−356.
29. Goormaghtigh, E., Cabiaux, V., and Ruysschaert, J. M. (1990) *Eur. J. Biochem. 193*, 409−420.
30. Cabiaux, V., Brasseur, R., Wattiez, R., Falmagne, P., and Ruysschaert, J. M. (1989) *J. Biol. Chem. 264*, 4928−4938.
31. Goormaghtigh, E., Vigneron, L., Scarborough, G., and Ruysschaert, J. M. (1994) *J. Biol. Chem. 269*, 27409−27413.
32. Goormaghtigh, E., and Ruysschaert, J. M. (1994) *Spectrochim. Acta 50A*, 2137−3144.
33. de Jongh, H. H., Goormaghtigh, E., and Ruysschaert, J. M. (1995) *Biochemistry 36*, 172−179.

34. Lakowitz, J. R. (1983) in *Principles of Fluorescence Spectroscopy*, Plenum Press, New York.
35. Sharom, F. J., Yu, X., and Doige, C. A. (1993) *J. Biol. Chem. 268*, 24197−24202.
36. Shapiro, A. B., and Ling, V. (1995) *J. Biol. Chem. 270*, 16167−16175.
37. Hooijberg, J. H., Pinedo, H. M., Vrasdonk, C., Priebe, W., Lankelma, J., and Broxterman, H. J. (2000) *FEBS Lett. 469*, 47−51.
38. Urbatsch, I. L., Sankaran, B., Weber, J., and Senior, A. E. (1995) *J. Biol. Chem. 270*, 19383−19390.
39. Goodno, C. C., and Taylor, E. W. (1982) *Proc. Natl. Acad. Sci. U.S.A. 79*, 21−25.
40. Urbatsch, I. L., Sankaran, B., Weber, J., and Senior, A. E. (1995) *J. Biol. Chem. 270*, 26956−26961.
41. Rayment, I. (1996) *J. Biol. Chem. 271*, 15850−15853.
42. Amos, L. A., and Cross, R. A. (1997) *Curr. Opin. Struct. Biol. 7*, 239−246.
43. Mao, Q., Leslie, E. M., Deeley, R. G., and Cole, S. P. C. (1999) *Biochim. Biophys. Acta 1461*, 69−82.
44. Kast, C., and Gros, P. (1997) *J. Biol. Chem. 272*, 26479−26487.
45. Stride, B. D., Valdimarsson, G., Gerlach, J. H., Wilson, G. M., Cole, S. P. C., and Deeley, R. G. (1996) *Mol. Pharmacol. 49*, 962−971.
46. Challou, N., Goormaghtigh, E., Cabiaux, V., Conrath, K., and Ruysschaert, J. M. (1994) *Biochemistry 33*, 6902−6910.
47. Vigneron, L., Ruysschaert, J. M., and Goormaghtigh, E. (1995) *J. Biol. Chem. 270*, 17685−17696.
48. Sonveaux, N., Vigano, C., Shapiro, A. B., Ling, V., and Ruysschaert, J. M. (1999) *J. Biol. Chem. 247*, 17649−17654.
49. de Jongh, H. H., Goormaghtigh, E., and Ruysschaert, J. M. (1997) *Biochemistry 36*, 13603−13610.
50. de Jongh, H. H., Goormaghtigh, E., and Ruysschaert, J. M. (1997) *Biochemistry 36*, 13593−13602.

BI001043V